Trajectories of land and ocean primary productivity across the Arctic coastal margin and sensitivity to coastal sea ice decline

Cynthia Garcia[1,2]
ceidel2@uic.edu, cynthia.garcia@noaa.gov
Max Berkelhammer[1]
berkelha@uic.edu
Larry Stock[-3]
larry.v.stock@nasa.gov

[1]University of Illinois at Chicago, Department of Earth, and Environmental Sciences, Chicago, IL, 60607 USA, [2]National Oceanic and Atmospheric Administration, Silver Spring, MD 20910, USA, [3]Insight Global, Arlington, VA 22209, USA

Corresponding author: Cynthia Garcia (ceidel2@uic.edu)

Key Points:

- From 2003-2020, coastal land and ocean GPP increased by the same magnitude of 12% and is displaying a *Synchronized Positive Shift (SPS)*.
- This converging response seems to be a product of increasing open water conditions and water and nutrient availability as driven by general warming.
- Land and ocean GPP show strong synchrony over 4–5-year cycles, illustrating that coastal synchrony observed over decadal timescales is mirrored over interannual timescales.

Abstract

The rapidly warming Arctic and its effects on sea ice extent, hydrology, and nutrient availability influence terrestrial and marine carbon cycles in a number of interrelated ways. While these changes likely have shared effect on adjacent land and ocean systems, we often study them in isolation, making it difficult to understand response patterns and trajectories in these carbon cycle hotspots. Using almost two decades of remotely-sensed Gross Primary Productivity (GPP) in

Arctic coastal margins, we test how the magnitude and direction of change in productivity covary. We observed that coastal marine productivity is four times that of coastal tundra productivity in the pan-Arctic. From 2003-2020, GPP in both the coastal land and ocean increased by approximately 12%. This common trajectory seems to be a product of increasing open water conditions, increased terrestrial water balance, and nutrient availability as driven by the regional warming. On a sectoral scale, we proposed a Coastal Synchrony Index (CSI) to compare the rate of change of ocean productivity relative to land productivity and show that ocean productivity is increasing faster than land in *inflow margins* of Barents, Bering, and Okhotsk, *outflow margins* of Canadian Arctic Archipelago (CAA) and Greenland/Iceland, and in *interior margin* of Eurasia. Additionally, we see strong coherence between land and ocean GPP on 4–5-year cycles illustrating that coastal synchrony observed over decadal timescales is mirrored over interannual timescales. These cycles align with variations in open water duration, emphasizing the pivotal role of reducing shorefast ice on terrestrial and marine productivity trajectories.

1. Introduction

The rapid declines in Arctic sea ice extent, melting permafrost, warming, and changes in hydrology are influencing Arctic land and ocean carbon cycles in a number of interrelated ways (Irrgang et al., 2022; Post et al., 2013; Schuur et al., 2015; Carmack et al., 2015; Rawlins et al., 2010). While a changing cryosphere and longer ice-free growing season would likely have a shared influence on land and ocean productivity, we often study them in silos. Consequently, their long-term joint behavior is generally poorly understood despite the numerous ways that coastal land and ocean systems are affected by similar mechanisms. On the ocean side, dramatic increases in ice-free areas have been shown to positively affect phytoplankton primary production in the open ocean (Lewis et al., 2020). Increasing wind mixing from more frequent storms has also been ascribed to promote the resuspension and upwelling of nutrients to the euphotic zone (Zhang et al., 2010; Tremblay et al., 2015). At the same time, increasing surface ocean stratification due to the intensification of freshwater flux from river runoff, ice melt, and positive precipitation minus evaporation (P-E) can limit ocean primary productivity due to its control on the transfer of nutrients to the surface layers (Nummelin et al. 2016; McLaughlin & Carmack, 2010, Popova et al., 2012). With a continued

decrease in sea ice cover, a cloudier, wetter Arctic is also expected (Liu et al., 2012; McIlhattan, et al., 2020), which can reduce surface ocean primary production.

On the terrestrial side, observations across various spatial scales show both greening and browning trends across the Arctic (Bhatt et al., 2010; Epstein et al., 2018). The presence of these diverging trends reflects a combination of co-occurring processes including increases in precipitation (that can aid water-limited systems but also lead to water-logging), higher CO_2 and nutrient deposition (fertilization), warmer temperatures (2-4 times the global average rate) (Rantanen et al., 2022; England et al., 2021), and higher evaporative demand as well as novel biotic interactions such as shrub encroachment and pests (Kankaanpää, et al., 2020). These changes in tundra vegetation have critical impacts on coastal permafrost stability, hydrologic cycles, and the exchange of materials between land and ocean, leading to major changes in the biogeochemical cycling in both land and ocean systems.

Limited studies have focused on understanding the large-scale variability of adjacent land and ocean carbon cycle across the radically changing Arctic coast. As the site of major exchange of water and other materials, strong connections between near-shore marine ecosystems and coastal tundra productivity are expected. Additionally, most of the Arctic tundra biome is closely tied to the adjacent marine system because about 80% of it is within 100 km of the coastline (Walker et al., 2005; Minke et al., 2007). To provide a regional view of the heterogeneity and coherency in coastal carbon cycle changes, we assess concurrent estimates of gross primary production (GPP), i.e., total fixation of carbon by primary producers through photosynthesis along adjacent land and ocean systems. Since ground-based and in-situ estimates of primary production are sparse in the Arctic, especially along coastal areas, this study takes advantage of the inherent ability of remote sensing datasets to provide long-term continuous observations that cross both the land and ocean interface. Here, we present a generalized coastal trajectory classification scheme based on observed temporal primary productivity trends in adjacent land and ocean systems. Moreover, land and ocean GPP are also dependent on a complex collection of factors, most notably light availability (Leu et al., 2015; Frey et al., 2011), nutrients (Tremblay et al., 2015; Fernandez-Mendez et al., 2015), temperature (Bhatt et al., 2013), water limitations (Elmendorf et al., 2012), and the influence of large-scale teleconnections (Slagstad et al., 2011; Bhatt et al., 2010).

Understanding the covariability of these important parameters with primary production could elucidate the links and the nature of coherency between adjacent land and ocean, which can contribute to understanding the way Earth System models capture complex cross-system dynamics.

The Arctic coastal margins are also highly sensitive to the presence or absence of sea ice. We expect a strong link between coastal sea ice and productivity since shorefast ice provides a first-order control on the physical vulnerability of the coast to erosion and inundation (Barnhard et al., 2014). Shorefast ice is an important buffer from wave action and temperature for considerable portions of the year (Farquharson, et al., 2018), and thus affects the amount of energy available for coastal primary production. With the rapidly declining sea ice extent (with 2020 sea ice minima being the second lowest after 2012) (NSIDC, 2020) and increasing frequency and duration of warm winter air temperature events (Graham et al., 2017), it is anticipated that such changes will have significant ecological consequences. Assessing the simultaneous impact of decreasing coastal sea ice on productivity across the land and ocean interface is therefore necessary not just to understand land-ocean primary productivity trajectory and patterns, but to also help answer questions on how the coastal margins will evolve in a new Arctic climate. To analyze this, we investigate key factors that might be able to explain regional land-ocean GPP coherence. Ultimately, by characterizing these important yet largely unknown connections along the Arctic coastal interface and related feedbacks, we hope to better inform biogeochemical processes and models, especially in the face of accelerating rates of Arctic terrestrial carbon cycling (Jeong et al., 2018) and ice-free summers now projected in 2030 (Kim et al., 2023).

2. Data and Methods

2.1. Coastal Trajectory Assessment

Here, we analyze almost two decades of primary productivity data that are concurrently available over land and ocean in the Arctic. We use FluxSat v2.0 GPP product (Joiner & Yoshida, 2020) over land, which is based on a light-use efficiency model and trained using in-situ eddy covariance measurements. FluxSat is based on the MCD43C Bidirectional Reflectance Distribution Function

(BRDF)-Adjusted reflectance from the Moderate-resolution Imaging Spectroradiometer (MODIS) Terra and Aqua. Apart from providing daily gridded estimates of GPP at 0.05-degree resolution, FluxSat v2.0 has observations from March 2000 to present, providing valuable insights into trends and changes in GPP over time. The GPP on the ocean side is estimated from three distinct data products. The first one developed by Lewis & Arrigo (2020) (herein referred to as Lewis) was created to account for the unique bio-optical properties of Arctic waters. The Lewis daily gridded NPP data (with units of mg C m^{-2} d^{-1}) are available at four (4) km resolution from 2003 to 2020. Other global ocean Net Primary Productivity (NPP) estimates available are through the ocean productivity products of the Oregon State University available at either ~9 km (1080 x 2160 global grid) or ~18 km (2160 x 4320 global grid) spatial resolution from July 2002 to present. Data used here include the Vertically Generalized Production Model (VGPM) (Behrenfeld & Falkowski, 1997) and the Carbon-based Productivity Model (CbPM) (Westberry et al., 2008). The Lewis NPP data was estimated using updated chlorophyll-a concentration developed by using 501 concurrent measurements of in situ remote sensing reflectance and chlorophyll-a, gathered from 25 distinct cruises across the Arctic Ocean (Lewis, et al., 2020). The VGPM product utilizes a widely used algorithm for estimating ocean NPP at regional to global scales. It is based on the relationship between NPP and chlorophyll-a concentration in the water, and calculates NPP as a product of chlorophyll-a, maximum daily net primary production per unit of chlorophyll in a given water column, day length, and a volume function that accounts for the decreasing photosynthetic rates with depth due to light penetration. Lastly, the CbPM algorithm relates NPP with phytoplankton carbon biomass (estimated from particulate backscattering coefficients) and growth rates (estimated from chlorophyll-to-carbon ratios). The CbPM also estimates a spectrally-resolved attenuation of light through the euphotic zone, providing an estimate of light available for photosynthesis. To estimate GPP from the three ocean NPP products, we use a conversion factor based on empirical characterization of phytoplankton photosynthetic efficiency, wherein GPP was found to be 3.3 times greater than NPP (Halsey et al., 2010).

All of the land and ocean GPP products are presented with the common unit of g C m^{-2} d^{-1} and are gridded on the same SSM/I (Special Sensor Microwave/Imager) polar stereographic grid with 12.5 km spatial resolution using a drop-in-the-bucket binning procedure (Kwok, 2022; Jensen, 2006) on a monthly basis. All monthly primary productivity data from 2003 to 2020 that fall within 100

km of a coastline across the pan-Arctic are extracted using the Distance to the Nearest Coastline dataset of NASA (NASA OBPG & Stumpf, 2012). The choice of using a 100-km nearshore buffer is because the global average of the width of continental shelves ranges from about 50-100 km (Harris et al., 2014). Shelf seas are areas of extensive deposition due to their proximity to river systems that supply sediments to the continental margins. With this spatial extent, we assume to capture processes occurring within Arctic tidal rivers, tidal wetlands, estuaries, and continental shelves and highlight the signals influenced by land- and marine-derived materials and energy flow across the coastal interface (Ward et al., 2020). On land, we look at the same 100-km buffer to ensure that we are looking at similar areas adjacent to the shoreline. This area can provide primary production along permafrost-affected coasts upstream from estuaries. These transition zones, affected by both terrestrial and marine influences, possess distinct characteristics. By analyzing the 100-km strip on both sides of the coastline, we gain a comprehensive perspective of how terrestrial factors impact marine processes and vice versa. Additionally, our examination of GPP seasonality revealed that the selected spatial extent remains largely consistent, even when considering thresholds between 50 and 100 km.

To address the heterogeneity across the Arctic coastlines, we divided the study area into nine (9) sectors based on ocean basins (Comiso, 2015) and analyzed them separately. These sectors are shown in figure 1 and labeled as Eurasian, Amerasian, Bering, Barents, Canadian Arctic Archipelago (CAA), Baffin/Labrador (B/L), Greenland/Iceland (G/I), Hudson Bay, and Okhotsk. The color-coded shaded areas represent the 100-km spatial extent from the coastline towards the ocean

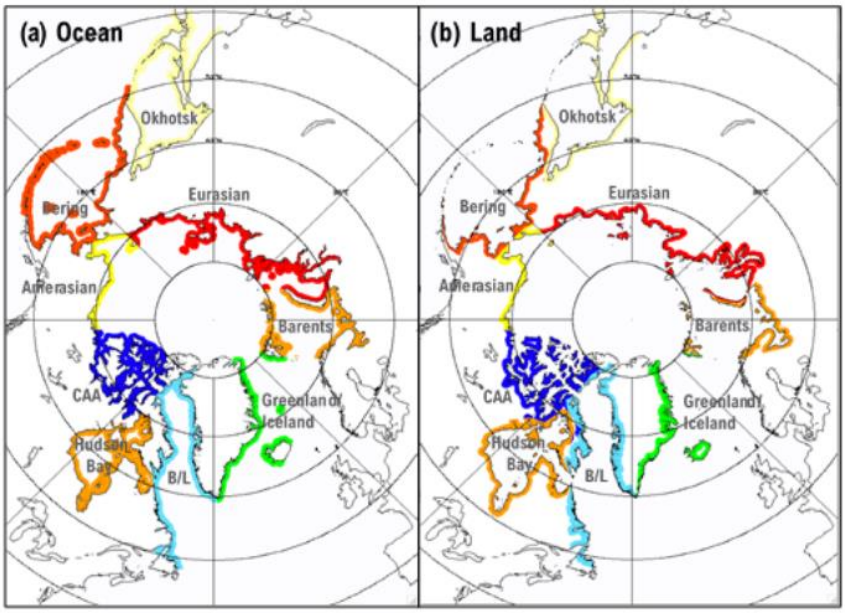

Figure 1. Nine Arctic coastal sectors. Color-coded areas represent the 100-km spatial extent from the coastline towards the (a) ocean and (b) land where data are collected. The nice sectors are Okhotsk, Bering, Eurasian, Barents, Greenland/Iceland, B/L, Hudson Bay, CAA, and Amerasian sectors (Comiso, 2015).

and towards land. The Eurasian sector covers the coastal regions along East Siberian, Laptev, and Kara Seas and is characterized by diverse Arctic ecosystems, including tundra, boreal forests, and coastal wetlands. The Eurasian sector experiences significant freshwater runoff from major Arctic rivers including the Ob, Yenisey, and Lena (Jakobsson, 2002). The Amerasian encompasses the coastal areas along North America and features tundra, taiga, and coastal plains. This region is dominated by the Beaufort Sea. It is impacted by the inflow of nutrient-rich waters from the Pacific Ocean and the large Mackenzie River (Carmack, E., et al., 2016). The Bering sector corresponds to the coastal regions around the Bering Sea, an area rich in marine biodiversity. The mixing of Pacific and Arctic waters in the Bering Sea creates a productive environment supporting a variety of marine life. Barents sector includes coastal areas along the Barents Sea and off the northern coasts of Norway and Russia. It is an important area for commercial fisheries and a site for the mixing of warm Atlantic water with colder Arctic water. Its coastline also experiences considerable reductions in sea ice cover from recent warming (Isaksen et al., 2022). The Canadian Arctic Archipelago (CAA) is a sector characterized by a series of large island groups in Northern Canada. It contains one-third of the global volume of land ice outside of Greenland and Antarctic ice sheets (Radic' & Hock, 2010). The Baffin/Labrador (B/L) sector includes the Baffin Bay and Labrador Sea, both notable for their interactions between glaciers and ocean currents. These waters are major sinks for atmospheric CO_2 being a region for deep water formation and primary production (DeGrandpre et al., 2006). The Greenland/Iceland (G/I) sector is characterized by its massive ice sheet in Greenland and meltwater coming from it as well as the volcanic landscapes of Iceland. Located in northeastern Canada, the Hudson Bay sector is a large inland sea connected to the Atlantic Ocean via the Hudson Strait. It is characterized by its seasonal ice cover and high freshwater input from large rivers. Lastly, the Okhotsk sector is off the coast of Russia's far east, separated from the Pacific by the Kuril Islands. The sector is notable for sea ice production, which drives ocean circulation and biogeochemical cycles (Nishioka et al., 2014).

We utilize a generalized coastal trajectory classification scheme based on observed temporal primary productivity trends in adjacent land and ocean systems. We call a coastal region with positive trends in both land and ocean primary productivity an area experiencing *Synchronized Positive Shift (SPS)*. For this classification, it is hypothesized that the same changes (e.g., warmer temperature, more rain, increased coastal open water days, and less snow) are positively affecting

both systems. For areas with both land and ocean primary productivity decreasing with time, we classify them as *Synchronized Negative Shift (SNS)* areas. In this scenario, common changes in sea ice cover, temperature, and water availability are negatively impacting both systems. This can emerge from factors such as higher evaporative demand leading to water stress for land plants and loss of habitat for primary producers in the sea ice. Areas with heavy and constant coastal erosion can also cause land GPP to decrease as well as carry particles and colored dissolved organic matter (cDOM) to adjacent marine systems that can cause increased turbidity, lessening ocean GPP. For conditions where land productivity is increasing while ocean productivity is decreasing or vice versa, it suggests a divergence in the trends. For the opposing trajectories, we have *Terrestrial-Dominant Shift (TDS)* and *Marine-Dominant Shift (MDS).* We characterize *TDS* as the scenario when land GPP increases, while ocean GPP decreases. Here, the same factors can cause opposite effects on adjacent systems. For example, warmer temperatures and more moisture can cause increases in land GPP. On the ocean side, however, warmer SST and increased freshwater flux from major Arctic rivers can cause lower ocean GPP with time due to stratification-induced nutrient limitation despite enhanced light transmission. For the *MDS* classification, ocean GPP increases while land GPP decreases. This can potentially occur due to increasing frequency of Arctic storms (Clow et al., 2011) that carry high winds and large amounts of rain that can potentially negatively affect land GPP through water-logging. Arctic storms are also most active in summer (Day & Hodges, 2018), which could reduce light availability and reduce GPP. On the ocean side, increasing windiness can potentially promote vertical mixing in the ocean and erode stratification, potentially promoting the upward delivery of new nutrients to the depleted euphotic zone as well as instigating secondary blooms in autumn. Strong winds can also expedite the breakup of sea ice, expanding the available open water area for photosynthesis. Lastly, we have the *No Change* scenario where neither land nor ocean are changing. Here, GPP remains constant and does not change with time. Apart from a generalized coastal trajectory classification scheme, we further categorize the sectors as either an *Interior margin* (Eurasian and Amerasian), which are coastal margins that are mostly influenced by the major Arctic rivers; *Inflow margin* (Bering, Okhotsk, and Barents), which are areas that are influenced by the inflow of warm, salty waters from the Pacific and Atlantic; and *Outflow margin* (CAA, B/L, G/I, and Hudson Bay), which are mostly influenced by cold, fresh water outflows from the Arctic Ocean (Carmack et al., 2006).

Annual and monthly aggregated time series for each sector were calculated and trends from monthly anomalies were determined using linear regression. The slope of the regression is considered significant for p values <0.05. Trends and total percent change for data from April to September (ice-free, productive periods on both land and ocean) from the years 2003-2020 are presented. On the ocean side, we only estimate GPP from open water areas or those with <15% sea ice concentration, and thus exclude primary production under or on sea ice. The 15% threshold is a standard definition used by the National Snow and Ice Data Center (NSIDC) to distinguish between ice-covered and ice-free areas (NSIDC, 2021). Spatial trends and estimates of land and ocean GPP from multi-year average in gC d^{-1} from 100 km landward and oceanward from the coastline in the Pan-Arctic (all coastal margins found at >60°N) are also presented. The months of peak primary productivity from the long-term dataset are also extracted to assess and compare seasonal variability and shifts in peak productivity on adjacent land and ocean domains. To evaluate coastal trajectory, we follow our proposed generalized classification scheme based on observed long-term primary productivity trends.

2.2. Coastal Trajectory Mechanisms

To investigate factors that might influence the observed Arctic coastal patterns of productivity, we assess the anomaly trends of key remotely sensed parameters that affect both land and ocean during the same study period. These include Land Surface Temperature (LST) -from the MODIS Aqua MYD11C3 version 6 data product (Wan et al., 2021), precipitation minus evaporation (P-E), runoff over land, P-E over the ocean, and upwelling favorable wind days from the European Centre for Medium-Range Weather Forecasts (ECMWF) Reanalysis 5 (ERA5) (Muñoz-Sabater, 2019). Upwelling favorable wind conditions were also assessed by looking at the number of days during the study period when winds were east/northeast parallel to the shelf break, and if alongshore wind speeds exceeded 5 m/s (Cury & Roy, 1989; Bakun, 1990). We assessed the number of open-water (OW) days using the Bootstrap version 2 (SB2) sea ice concentration data (Comiso et al., 2017) from the NSIDC. The duration of OW is defined here as the average number of days where the pixels are ice-free (<15% sea ice concentration). For consistency with the land and ocean primary productivity data sets used in this study, all temperature, P-E, OW days, and sea ice products were also gridded in the same polar stereographic grid with 12.5 km resolution on a monthly basis.

We focus on changes in temperature, water availability, coastal sea ice conditions, and upwelling favorable wind days because these are key essential variables that affect both land and ocean systems on our time scale of interest. Temperature affects the metabolic rates of photosynthesizing organisms (both terrestrial plants and marine phytoplankton), influencing their growth rates and, consequently, primary productivity (Clarke & Gaston, 2006). On land, water availability directly impacts plant growth and productivity (Rodriguez-Iturbe, 2000). In the ocean, freshwater inputs from rivers or melting sea ice can affect the stratification of the water column, nutrient availability, and light penetration, all of which can influence phytoplankton productivity (Garcia, et al., 2021; Arrigo & van Dijken, 2004). Coastal sea ice and OW conditions affect light availability for phytoplankton growth and influence nutrient dynamics by its seasonal melting and freezing processes (Leu et al., 2015). These three variables are also interconnected and can influence each other, resulting in compounded effects on coastal primary productivity (Post et al., 2009). Just like with the coastal trajectory assessment of primary productivity, the temperature, water availability, OW conditions as well as upwelling favorable wind days were evaluated using data from 2003-2020 within the 100 km from the coastline to land and ocean from the pan-Arctic (>60°N) and the nine sectors. Other variables analyzed were instantaneous nutrient export from major Arctic river monitoring gauges. We acknowledge that in the surface ocean, primary production is limited by the availability of key nutrients such as nitrogen, phosphorus, and iron. While this is important, data available on a regional scale are scarce and are limited to point measurements typically around the mouths of major Arctic rivers making the characterization of nutrient limitations challenging. It is worth noting, however, that although we did not directly assess nutrients, we used indicators like runoff and upwelling as proxies to infer nutrient limitation on GPP.

To compare changes in land-ocean primary productivity with changes in temperature, water availability, and coastal OW conditions we estimate a Coastal Synchrony Index (CSI). The CSI is defined here as the quotient of the rate of change in ocean GPP over the rate of change in land GPP for each of the sectors. This ratio represents the rate of change of ocean productivity relative to the rate of change of land productivity and can offer insights into how marine and terrestrial productivity are related. If the CSI is greater than 1, it suggests ocean productivity is changing at a faster rate than land productivity. If the ratio is less than 1, it indicates that ocean productivity is

changing at a slower rate than land productivity. A ratio of 1 implies that both are changing at the same rate. The CSI can be a valuable metric in understanding the relative dynamics of change between land and ocean productivity, potentially revealing important ecological trends and interactions between the two environments. We then assess the correlation of the CSI values with changes in temperature, water availability, and coastal OW conditions in the nine sectors and in the Pan-Arctic. This analysis is intended to reveal how changes on said parameters may be driving changes in productivity patterns across the different geographical sectors. From the results of the pairwise plots with regression lines, we identified the key predictors and evaluated their contribution to the variability in CSI. We created a multiple linear regression model and to illustrate its skill, compared the predicted with the observed CSI values.

Lastly, to investigate the interconnected dynamics of land and ocean GPP and coastal sea ice conditions across the pan-Arctic region, we employ wavelet coherence analysis, using the 'WaveletComp' package in R (Rösch & Schmidbauer, 2018). The wavelet technique analyzes periodic phenomena in time series data by decomposing a time series into time-frequency space. It gives information about the dominant modes of variability and how the modes vary in time (Torrence & Compo, 1998). Through wavelet coherence analysis we highlight time periods where two time series co-move at a specific frequency, and can detect if the two series have common cycles. Since the WaveletComp package can only process data without gaps, we use seasonally decomposed missing value imputation for the missing data during non-productive months using the ‘imputeTS’ package in R (Moritz & Bartz-Beielstein, 2017). This method works well for data with both trend and seasonality. The wavelet and cross-wavelet analysis of land and ocean primary productivity, in conjunction with pan-Arctic OW days, will assess the influence of coastal ice conditions—a unique and significant driver of primary productivity on these adjacent ecosystems. More information on the 'WaveletComp' package can be found in its documentation and the work of Roesch & Schmidbauer (2018).

3. Results

In terms of the magnitude and timing of peak productivity along the Arctic coastlines, it is observed that across the pan-Arctic, the marine grid cells had a cumulative GPP of 1.25×10^{-5} Pg C yr^{-1}

when using the Lewis product, whereas the land grid cells had a total of 3.06 x 10^{-6} Pg C yr^{-1}. This indicates that the pan-Arctic coastal marine areas are approximately four (4) times larger or have 300% greater GPP than land when considering data in the last two decades. In terms of timing of peak productivity, the results in figure 2a show a latitudinal effect in period of peak productivity, especially in the marine component, with later peaks observed in higher northern latitudes. This is also seen in the plots in figure 2b where the marine component (blue) is observed to be shifting to the right with increasing latitude. On land, we see a bimodal distribution with peaks in June and July. The cumulative frequency distribution plots in figure 2c highlight the divergence of the timing of peak primary productivity with marine component peaking later in the year. These later peaks on the ocean side are more pronounced along Eurasian and the CAA coastal zones.

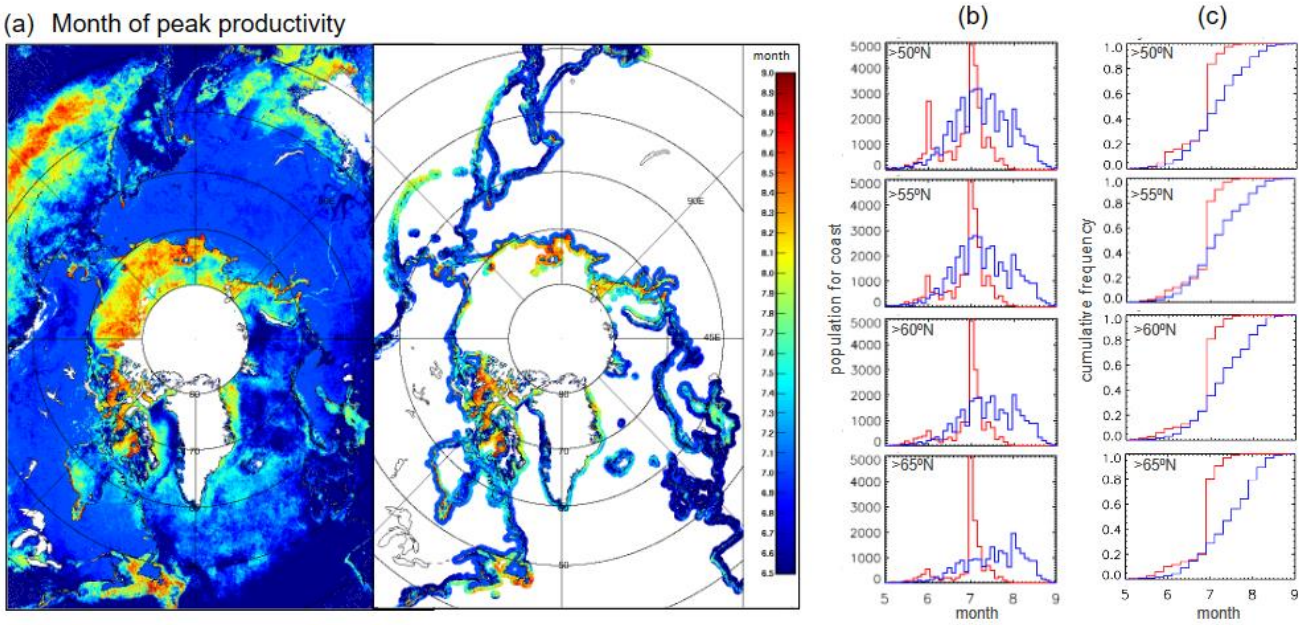

Figure 2. (a) Left panel - map of pan-Arctic peak month productivity on both land and ocean; Right panel - peak month productivity in our study area, 100 km from the coastal margins on land and ocean. (b) Histogram of peak month productivity extracted from >50°N, >55°N, >60°N, and >65°N of the study area. (c) cumulative distribution frequency of peak month productivity from >50°N, >55°N, >60°N, and >65°N of the study area. For both (b) and (c), the blue line corresponds to marine data, while red is for land.

In terms of seasonal climatology of coastal productivity, figure 3a shows average data during spring and early summer (April-June) and summer and early autumn (July-September) in figure 3b for land GPP and the three marine GPP products. High primary productivity is observed along the mouths of major Arctic rivers (locations are shown in the first panel with black arrows) across the different marine GPP products. However, a more conservative concentration and distribution are observed in the Lewis product compared to CbPM and VGPM. The relationship between the

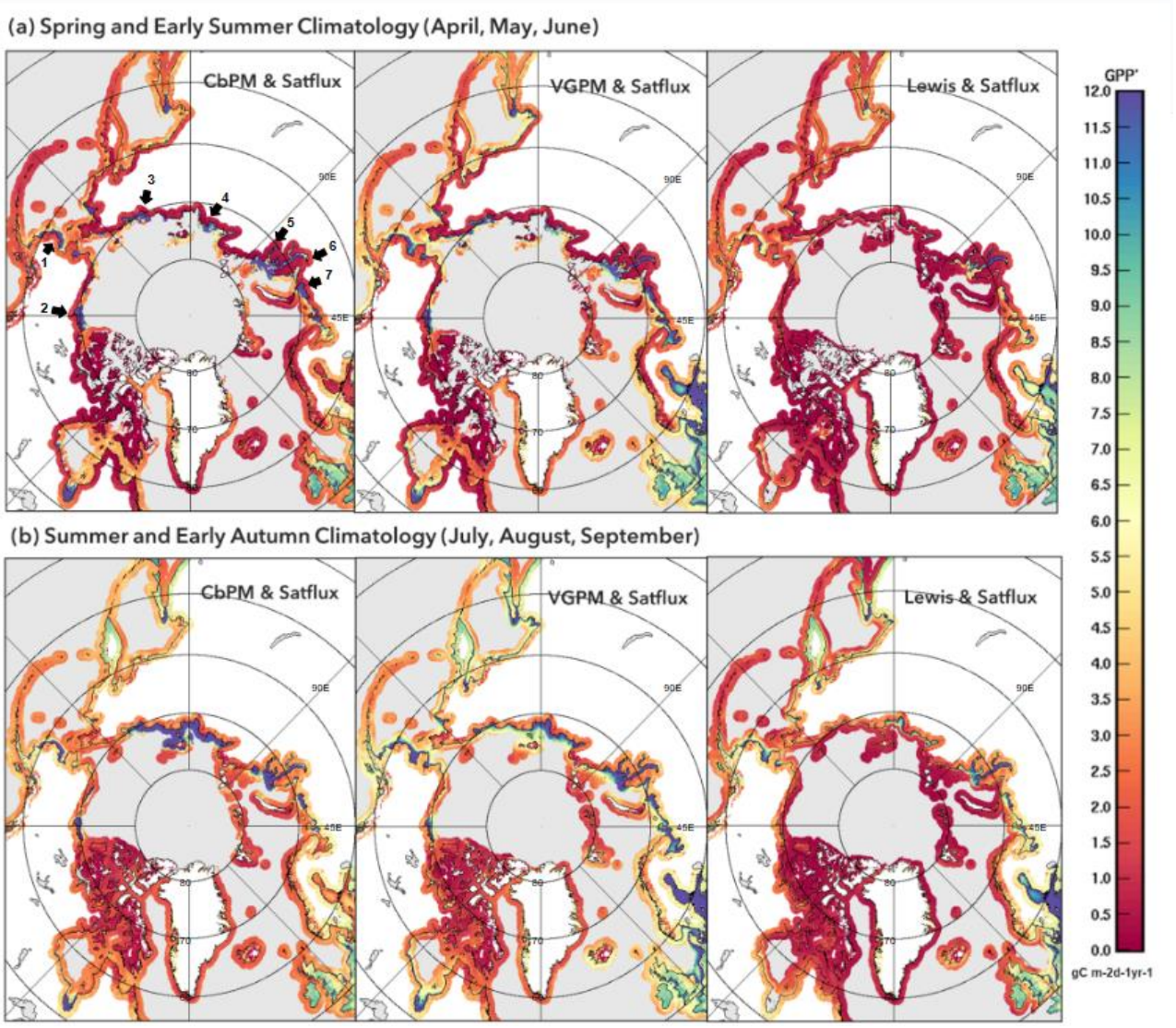

Figure 3. Seasonal climatology of land and ocean primary productivity in the study area. (a) spring and early summer climatology for the months April-June from 2003-2020 for FluxSat land GPP and the three ocean productivity products: CbPM, VGPM, and Lewis. (b) summer and early autumn climatology for the months July-September from 2003-2020 for the same land and ocean primary productivity products. Black arrows on the first panel show the location of the mouths of major Arctic rivers, namely (1) Yukon (2) Mackenzie, (3) Kolyma, (4) Lena, (5) Yenisey, (6) Ob, and (7) Pechora.

timing of sea ice melt and marine primary productivity is more evident in figure 3b. At the height of summer and early autumn, sea ice completely disconnects from the shoreline exposing open ocean areas for photosynthesis causing the distinct peaks of GPP. There is also the contribution from the highly seasonal delivery of nutrients from rivers and coastal erosion (Terhaar et al., 2021). The adjacent coastal tundra on -another hand, though modest, shows increasing productivity after snowmelt in spring and early summer. Productivity values then increase towards peak values in July and August. In terms of distribution, the Arctic coastal tundra shows changes in the spatial distribution of vegetation across north-south climate gradients (Raynolds et al., 2019).

Table 1. Total percent change, land and ocean GPP anomaly trends, and coastal trajectory classification in the Pan-Arctic and nine sectors from the 18-year time series (2003-2020). Significant trends ($p < 0.05$) are in bold.

	Land GPP (% change)	Ocean GPP (% change)			Land GPP Trend (gC m-2d-1yr-1)	Ocean GPP Trend (gC m-2d-1yr-1)			Classification
		CbPM	VGPM	Lewis		CbPM	VGPM	Lewis	
Pan-Arctic	12.625	5.766	11.677	11.510	**0.010**	-0.004	**0.065**	**0.018**	**SPS**
Eurasian	24.944	-16.760	-8.959	27.152	**0.015**	0.024	**0.237**	**0.027**	**SPS**
Amerasian	38.868	-15.739	-14.226	-20.067	**0.011**	0.037	**0.029**	-0.001	TDS
CAA	18.808	3.253	19.304	22.802	**0.013**	-0.129	**0.065**	**0.034**	**SPS**
Okhotsk	7.886	3.313	31.009	19.894	**0.026**	-0.009	0.013	**0.005**	**SPS**
Bering	15.879	12.634	18.081	9.949	**0.021**	0.009	**0.035**	**0.026**	**SPS**
Barents	11.327	-1.435	0.315	28.396	**0.009**	-0.020	**0.070**	**0.036**	**SPS**
Greenland/Iceland	-7.326	22.887	-0.407	4.443	0.005	0.010	**0.013**	0.006	SPS
Hudson Bay	5.267	-22.154	12.672	10.266	0.002	0.007	-0.001	0.005	SPS
Baffin/Labrador	7.431	-5.885	-11.524	-11.273	-0.002	-0.002	0.009	0.003	MDS

In terms of primary productivity trajectory and magnitude of change through time, we found that primary productivity over land has increased by about 13% in the pan-Arctic between 2003 and 2020 with 0.010 gC m^{-2} d^{-1} added each year (Table 1) or 3,650,000 gC km^{-2} y^{-1}. Ocean primary productivity has also increased by a range of about 12% if using the Lewis data and VGPM, and 6% if using CbPM in the pan-Arctic. Rates of change are 0.018 gC m^{-2} d^{-1}, 0.065 gC m^{-2} d^{-1} and -0.004 gC m^{-2} d^{-1} when using Lewis, VGPM, and CbPM respectively, although only Lewis and VGPM trends are statistically significant. An overall *Synchronized Positive Shift (SPS)* in pan-Arctic primary productivity was observed when analyzing coastal margins with the VGPM and Lewis marine data and FluxSat land data. On a regional level, the Eurasian, Canadian Arctic Archipelago (CAA), Okhotsk, Bering, Amerasian, and Barents sectors showed statistically

significant *SPS* patterns on both land and sea when using VGPM and Lewis trends on the ocean component. Although statistical significance was found only on land, the Amerasian sector demonstrated a *Terrestrial Dominant Shift (TDS)* when considering Lewis data.

A closer look at the rates of primary productivity on land shows that the steepest greening rates are observed along the North Pacific *inflow margins* of Okhotsk (0.026 gC m^{-2} d^{-1} y^{-1}) and Bering (0.021 gC m^{-2} d^{-1} y^{-1}). This is followed by Eurasia at 0.015 gC m^{-2} d^{-1} y^{-1}. Other sectors in order of decreasing land GPP rates are CAA at 0.013 gC m^{-2} d^{-1} y^{-1}, Amerasian at 0.011 gC m^{-2} d^{-1} y^{-1}, Barents at 0.009 gC m^{-2} d^{-1} y^{-1}, Greenland/Iceland at 0.005 gC m^{-2} d^{-1} y^{-1}, and Hudson Bay at 0.002 gC m^{-2} d^{-1} y^{-1}. Baffin/Labrador, which is an *outflow margin,* is experiencing browning on land at a rate of -0.002 gC m^{-2} d^{-1} y^{-1} although this trend is not statistically significant. In terms of percent change, Amerasian has the highest change during the study period at about 39% increase, followed by Eurasian at 25%, CAA at 19%, Bering at 16%, Barents, at 11%, Okhotsk at 8%, B/L at 7%, and Hudson Bay at 5%. The G/I sector is the only sector that displays a decreasing land primary productivity from 2003 to 2020 at -7%. On the ocean side, the CbPM monthly anomaly trends show decreasing productivity, although values are not statistically significant. The Lewis data and VGPM show similar increasing productivity across the pan-Arctic at 0.018 gC m^{-2} d^{-1} y^{-1} and 0.065 gC m^{-2} d^{-1} y^{-1}, respectively. For the VGPM data, the steepest statistically significant increase is observed along the Eurasian nearshore margins at a rate of 0.237 gC m^{-2} d^{-1} y^{-1}, followed by Barents at 0.070 gC m^{-2} d^{-1} y^{-1}, CAA at 0.065 gC m^{-2} d^{-1} y^{-1}, Bering at 0.035 gC m^{-2} d^{-1} y^{-1}, Amerasian at 0.029 gC m^{-2} d^{-1} y^{-1} and G/I at 0.013 gC m^{-2} d^{-1} y^{-1}. For the Lewis data, the steepest statistically significant increase is observed along the Barents nearshore margins at a rate of 0.036 gC m^{-2} d^{-1} y^{-1}, followed by CAA at 0.034 gC m^{-2} d^{-1} y^{-1}, Eurasian at 0.027 gC m^{-2} d^{-1} y^{-1}, Bering at 0.026 gC m^{-2} d^{-1} y^{-1} and Okhotsk at 0.005 gC m^{-2} d^{-1} y^{-1}. The only coastal marine sector that is showing a negative rate is Amerasian at -0.001 gC m^{-2} d^{-1} y^{-1}, though not statistically significant.

The spatial distribution of Arctic coastal trajectories is highlighted in the GPP trend maps in Figure 4. The coastal primary productivity trends in gC m^{-2} d^{-1} y^{-1} are shown for marine GPP products, VGPM and Lewis, and land GPP product, FluxSat, with areas with greens showing increasing productivity, and areas with maroons showing decreasing productivity with time. While there are several local-scale “hotspots” present in the data, we focus instead on the sectoral trends and

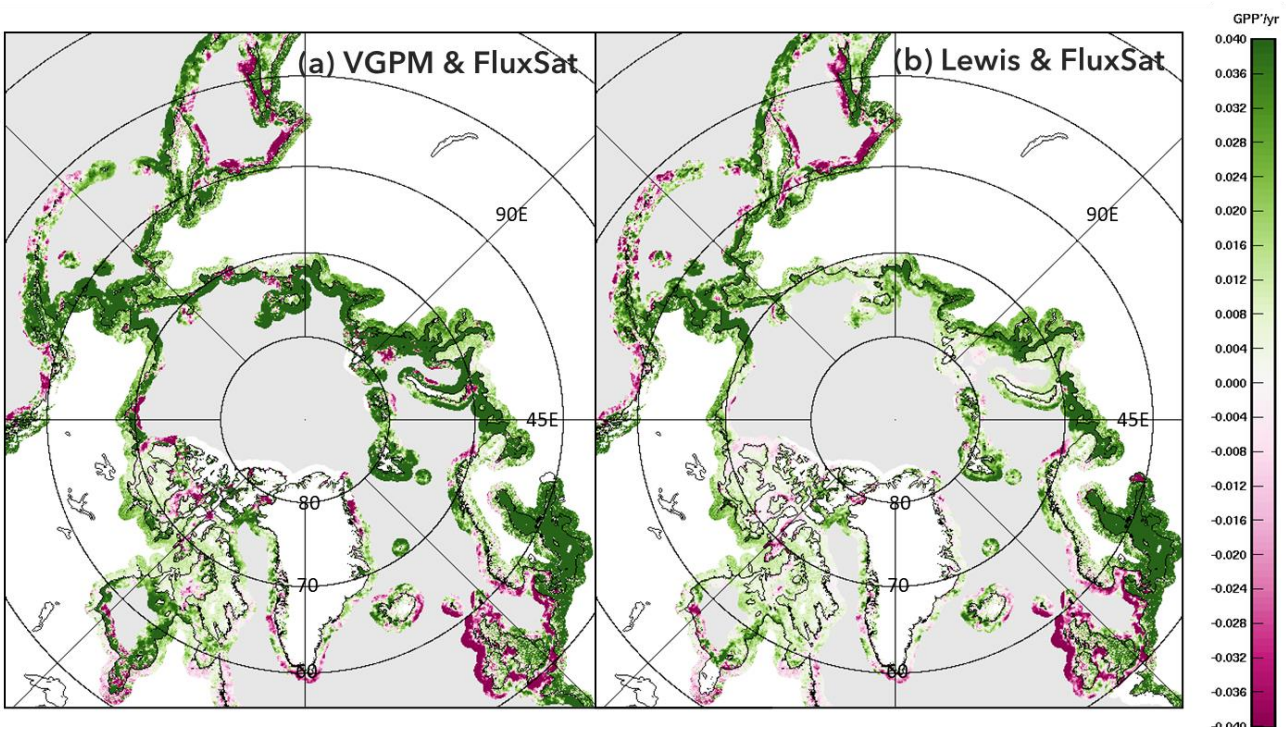

Figure 4. Land and Ocean GPP trends in gC m-2 d-1 y-1 from 100 km from coastline towards land and 100 km towards the ocean from 2003-2020 using (a) VGPM and Fluxsat, and (b) Lewis and FluxSat.

regional changes. Figure 4a using VGPM shows some decreasing productivity along some major river mouths, but also intense blooms (greens) in most sectors. Figure 4b with Lewis data highlights the convergence, specifically, an *SPS* type of synchrony observed using sectoral trends. Unlike VGPM, the Lewis trends are more positively conservative. This could be due to the corrections made by the authors to account for the unique bio-optical conditions of Arctic waters.

To explore the potential mechanisms driving the prominent patterns of convergence across the pan-Arctic coasts, we assess changes in temperature, hydrology, and coastal sea ice conditions. Table 2 summarizes the monthly anomaly trends in LST (°C yr^{-1}), P-E (m yr^{-1}), and Runoff (m yr^{-1}) over land as well as changes in SST (°C yr^{-1}), P-E (m yr^{-1}), and OW days (d yr^{-1}) over the ocean. Also included are the land and ocean (Lewis product) GPP trends in the pan-Arctic and the nine sectors. Over the almost two decades of data, we observe positive trends in LST at 0.053 °C yr^{-1}, SST at 0.018 °C yr^{-1}, and P-E over land (0.005 m yr^{-1}) and ocean (0.007 m yr^{-1}). The ice-free condition in the pan-Arctic is also increasing at 0.152 d yr^{-1}. Statistically significant positive LST trends occurred in the Eurasian, Okhotsk, and Bering sectors. The steepest positive trend for LST

Table 2. Trajectories of land and ocean productivity in the Pan-Arctic and nine sectors, based on FluxSat and Lewis. Trends of LST, P-E, and Runoff on land, and SST, P-E, OW Days, and Upwelling Favorable Wind Days over the ocean from 2003-2020. Significant trends ($p < 0.05$) are in bold.

	Land GPP Trend gC m-2d-1yr-1	Ocean GPP Trend gC m-2d-1yr-1	Land			Ocean			
			LST (°C yr-1)	P-E (m yr-1)	Runoff (m yr-1)	SST (°C yr-1)	P-E (m yr-1)	OW Days (d yr-1)	Upwelling Wind (d yr-1)
Pan-Arctic	**0.010**	**0.018**	**0.053**	**0.005**	0.0003	**0.018**	**0.007**	**0.152**	**0.0524**
Eurasian	**0.015**	**0.027**	**0.146**	0.005	0.006	**0.047**	**0.009**	**0.291**	**0.0289**
Amerasian	**0.011**	-0.001	0.039	0.007	-0.007	0.013	0.006	**0.114**	**0.0237**
CAA	**0.013**	**0.034**	0.051	**0.017**	-0.003	0.022	**0.019**	**0.005**	-0.0005
Okhotsk	**0.026**	**0.005**	**0.047**	0.009	-0.003	**0.035**	0.012	**0.042**	**0.0213**
Bering	**0.021**	**0.026**	**0.069**	0.012	0.006	**0.047**	0.008	**0.084**	**0.0306**
Barents	**0.009**	**0.036**	0.044	0.009	**0.013**	**0.036**	0.011	**0.263**	**0.0218**
Greenland/Iceland	0.005	0.006	-0.017	0.017	0.002	0.001	0.018	**0.080**	**-0.1133**
Hudson Bay	0.002	0.005	0.0003	-0.010	**-0.012**	-0.001	-0.004	0.019	0.13534
Baffin/Labrador	-0.002	0.003	0.005	-0.008	-0.008	-0.012	-0.005	-0.005	-0.0863

is found in the Eurasian (0.146 °C yr^{-1}), followed by Bering (0.069 °C yr^{-1}) and Okhotsk (0.047 °C yr^{-1}). For SST, statistically significant increases are observed along the Eurasian, CAA, Okhotsk, Bering, and Barents sectors. The steepest statistically significant SST trends are observed along Bering and Eurasian both at 0.047 °C yr^{-1}, followed by Barents (0.036 °C yr^{-1}) and Okhotsk (0.035 °C yr^{-1}). For P-E over both land and ocean, we observe increasing trends, except along Hudson Bay and Baffin/Labrador sectors. In terms of runoff, statistically significant trends are observed along Barents (0.013 m yr^{-1}) and Hudson Bay (-0.012 m yr^{-1}). For upwelling favorable winds, a general increase in days when winds blow parallel to the coast is observed in the pan-Arctic (0.052 d yr^{-1}). Trends in decreasing order are observed along Bering (0.031 d yr^{-1}), Eurasian (0.029 d yr^{-1}), Amerasian (0.052 d yr^{-1}), Barents (0.022 d yr^{-1}), and Okhotsk (0.021 d yr^{-1}).

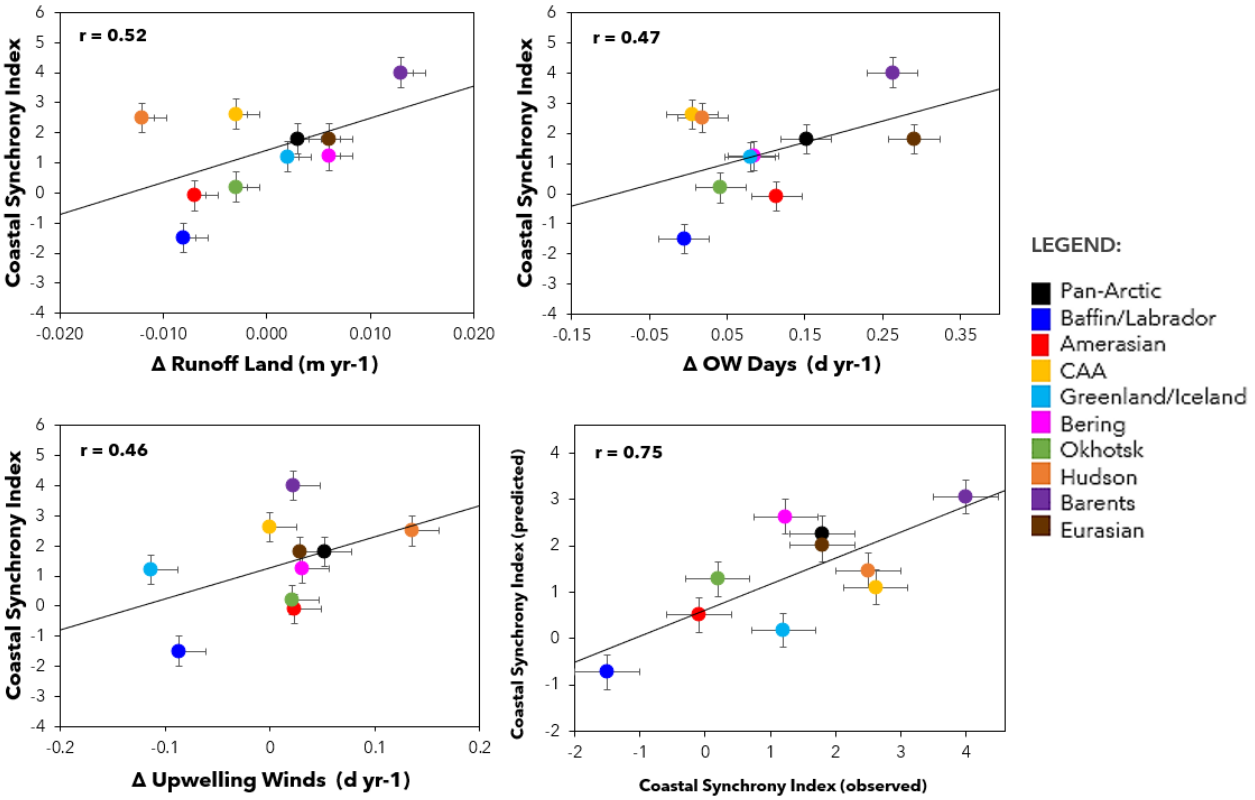

Figure 5. Relationship of changes in Runoff (m yr-1), Open Water (OW) days (d yr-1), Upwelling favorable wind days (d yr-1) vs Coastal Synchrony Index (CSI) based on FluxSat and Lewis data in the pan-Arctic and nine sectors. Error bars are confidence limits on the mean based on bootstrap resampling. The bottom right figure shows observed values of CSI vs predicted values of CSI using a multi-linear regression model including runoff, OW days, and Upwelling wind days as drivers.

Interestingly, G/I sector is experiencing decreasing upwelling favorable wind days at -0.113 d yr^{-1}. Lastly, positive trends in OW days occurred in all regions except in the Baffin/Labrador sector. The steepest statistically significant increase in open water conditions can be seen in the Eurasian coastal margin (0.291 d yr^{-1}), followed by Barents (0.263 d yr^{-1}), Amerasian (0.114 d yr^{-1}), Bering (0.084 d yr^{-1}), Greenland/Iceland (0.080 d yr^{-1}), Okhotsk (0.042 d yr^{-1}), and CAA (0.005 d yr^{-1}). Overall, we observe a general warming trend on both land and ocean, increasing water availability through a positive P-E, and a decreasing sea ice condition across the pan-Arctic coastal margins.

When comparing the CSI with changes in other parameters, we find that changes in runoff, OW days, and upwelling favorable wind days all have explanatory power with respect to the spatial (i.e., basin to basin) CSI values. To compute the CSI values in these plots, we used the monthly anomaly trends of FluxSat and Lewis products because the Lewis product was developed as an Arctic-specific algorithm to help improve estimates of chlorophyll-a, colored dissolved organic matter (cDOM) absorption, and particle backscattering in the Arctic Ocean (Lewis & Arrigo,

2020). As illustrated in figure 5, increasing rates of runoff, OW days, and upwelling favorable wind days are positively correlated with the ratio of change in ocean and land productivity. This indicates that the coastal productivity in the ocean is responding faster than land to the increase in OW days, upwelling wind days, and runoff. Sectors with CSI values greater than 1, namely Barents (4.0), CAA (2.6), Hudson (2.5), Eurasian (1.8), Bering (1.2), G/I (1.2), and Okhotsk (0.19) suggest that ocean productivity is changing at a faster rate than land productivity in these coastal areas, while also displaying a *Synchronized Positive Shift (SPS)* type of coastal productivity trajectory. Amerasian (-0.09) and B/L (-1.5) sectors have CSI values less than 1, which indicates that ocean productivity is changing at a slower rate than land productivity in these areas. The pan-Arctic has a CSI value of 1.8 suggesting that ocean primary productivity might be changing faster than land and that the two systems are significantly influenced by disappearing coastal sea ice, increasing upwelling favorable wind days, and transport of water over land. Employing a multiple linear regression model including runoff, OW days, and upwelling favorable wind days we could explain approximately 76% of the basin-to-basin variations in CSI.

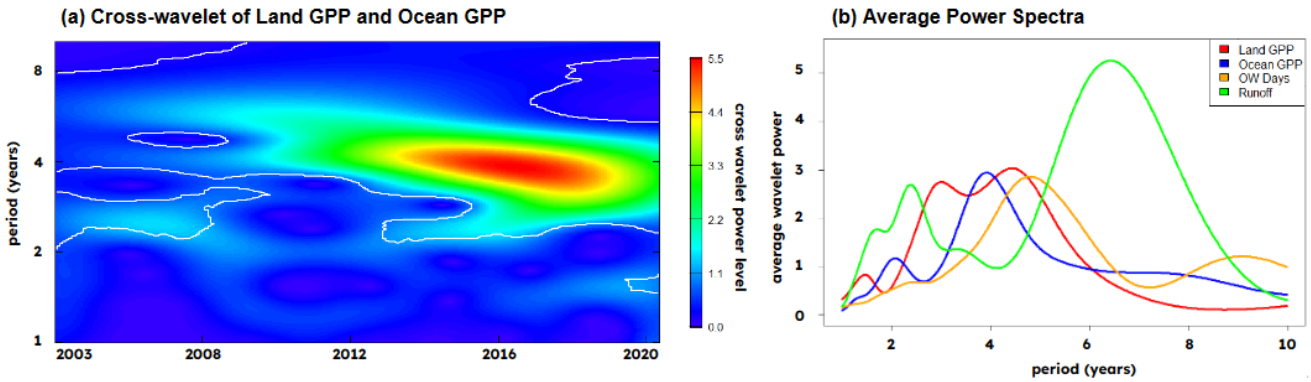

Figure 6. (a) Cross-wavelet transformation of land GPP and ocean GPP in the pan-Arctic using FluxSat and Lewis. White contours represent regions where the observed patterns are statistically significant at the 2.5% level; and (b) Wavelet power spectra of land GPP (red), ocean GPP (blue), OW days (orange), and runoff (green).

Decomposing ocean GPP and land GPP into the time-frequency space and looking at their cross-wavelet transformation in figure 6a and b shows that the adjacent land-ocean systems share a common dominant period of 4-5 years. This demonstrates that the synchrony we observed from previous analysis over decadal timescales is mirrored by synchrony on higher frequency timescales. The ocean GPP (blue) contains a persistent cycle of about 4 years, while the land GPP (red) contains a dominant period of 3-5 years. The OW days (orange) on the other hand also show a dominant period between 4-5 years. This shared 4–5-year period between land and ocean GPP

appears to be synchronized with a significant 4-5-year natural oscillation of sea ice in polar areas as also observed by Scafetta & Mazzarella (2015). It is also interesting to note that runoff (green) seems to have a dominant period of 7 years and 2 years. These results could indicate that OW days drive land-ocean GPP synchrony on interannual timescales, while the role of runoff is occurring more strongly over longer timescales.

4. Discussion

Understanding large-scale changes in GPP is crucial in identifying key patterns and processes that promote or inhibit a region's capacity to act as a carbon sink and its vitality as an ecosystem (e.g. declines in GPP may mark susceptibility to disturbances). On the pan-Arctic scale, sustained transformation to a less frozen state has been shown to increase Arctic open ocean NPP by more than 50% between 1998 and 2018 (Lewis et al., 2020). Local-scale estimates however vary depending on sea ice conditions and changing wind patterns (Manizza et al., 2019). The current projected change of Arctic ocean NPP also has a large range, going from a reduction of -25% to an increase of 60% (Vancoppenole et al., 2013) making the determination of not only the amplitude but even the sign of change uncertain. In low-stature coastal tundra environments, vegetation also displays spatially and temporally variable patterns of greening and browning (Frost et al., 2020; Bhatt et al., 2010; Epstein et al., 2018; Stow et al., 2004). Along the coastal regions, which are areas that provide a disproportionate contribution to the global and regional- primary production and carbon storage (Chen & Borges, 2009; Muller-Karger et al., 2005), changes and trajectories of the total photosynthetic CO_2 fixation are quite unknown due to the dearth of studies that consider the marine and terrestrial systems simultaneously. Here we leveraged almost two decades of remotely sensed primary production measurements targeted along the Arctic coastal margins to understand shared spatial and temporal patterns across adjacent terrestrial and marine domains. These are areas of some of the most biologically and geochemically active systems on Earth (McNicol et al., 2023).

The magnitude of primary production in Arctic coastal margins reveals distinctively higher marine productivity, surpassing that of the tundra environments by four times. Marine systems, particularly coastal zones, are highly dynamic and can rapidly respond to environmental changes,

such as extended periods of sunlight as well as nutrient availability following sea ice melt. Terrestrial systems, in contrast, are often constrained by snow cover, the slow thawing of permafrost and shorter growing seasons (Bhatt et al., 2014). Terrestrial environments in the Arctic are also often characterized by less biodiversity and biomass, with plant communities that are adapted to withstand harsh conditions rather than maximize growth (Post et al., 2009; Reynolds & Tenhunen, 1996; Zimov et al., 2006; Schuur et al., 2008). On the timing, the observation that peak productivity in coastal marine zones occurs later than in coastal land areas further north can be attributed to the timing of ice melt, which control available light (Arrigo et al., 2008), nutrient availability (Tremblay et al., 2015), and temperature effects (Steele, 2004). Some marine primary producers might also require a longer period of favorable conditions to initiate their peak productivity phase (Kahru et al., 2011). The divergence in the period of peak month productivity between adjacent marine and terrestrial regions is most evident in the CAA and Eurasia which could potentially be due to longer-lasting sea ice in these regions relative to other parts of the Arctic (Serreze and Stroeve, 2015) as well as from water column stability influenced by river runoff. On land, the bimodal distribution with peaks in June and July shows the shifting of vegetation from early blooming species to those that flourish in the warmer, later parts of the summer (Zhang et al., 2013). For example, dwarf shrubs and sedges peak early in the season, while graminoids and forbs continue to photosynthesize into the late summer, leading to this bimodal pattern. This shift can be indicative of the adaptations and phenological shifts occurring in response to changing climatic conditions (Post et al., 2009). While marine systems may show higher primary productivity levels as well as later and longer peak conditions compared to land, it is important to note that the two systems are closely interconnected. Changes in one can influence the other, particularly in a rapidly warming Arctic. Furthermore, an essential facet of the timing pertains to its implications for observed seasonal cycles of atmospheric CO_2. Regions that synchronize terrestrial and marine productivity might experience short yet intense intervals of CO_2 drawdown (Berkelhammer, 2019). Conversely, regions with disjointed land-sea productivity peaks might display an extended yet less pronounced CO_2 drawdown. Understanding these nuances in both the timing and magnitude of marine and terrestrial GPP is useful, especially when interpreting long-term CO_2 records from monitoring stations like in Utqiaġvik (formerly known as Barrow), Alaska and Alert, Canada.

Assessing the potential mechanisms behind the observed convergence and increasing primary productivity over land (13%) and ocean (12% and 6%) from 2003 to 2020 across the pan-Arctic coasts highlights a set of interconnected processes related to climatic changes. The phenomena of *Synchronized Positive Shift (SPS)* in both terrestrial and marine environments across the Arctic coasts seem to indicate the effects of Arctic amplification or increased regional warming (Serreze and Barry, 2011). This dynamic is illustrated in figure 7 which shows a representation of before (top) and after (bottom) observed warming and a corresponding increase in OW conditions, upwelling favorable wind days, and runoff along the Arctic coasts. In recent years, high OW conditions result in a warmer, wetter, and more maritime coastal tundra region (Bhatt et al., 2021), which along with earlier snowmelt positively influences vegetation growth. The observed warming trends, with a positive change in land surface temperature (LST) of 0.053 °C yr-1 and sea surface temperature (SST) of 0.018 °C yr-1, are conducive to plant growth and phytoplankton blooms, as they often respond to temperature cues (Thomas et al., 2010; Wassmann et al., 2011). This is particularly evident in the North Pacific inflow margins of Okhotsk and Bering, which show the steepest greening rates. The increase in precipitation minus evaporation (P-E) over land (0.005 m yr^{-1}) and ocean (0.007 m yr^{-1}) indicates greater water availability over land and freshwater in the ocean, further acting to support productivity. Additionally, the trends towards increased runoff, like the significant

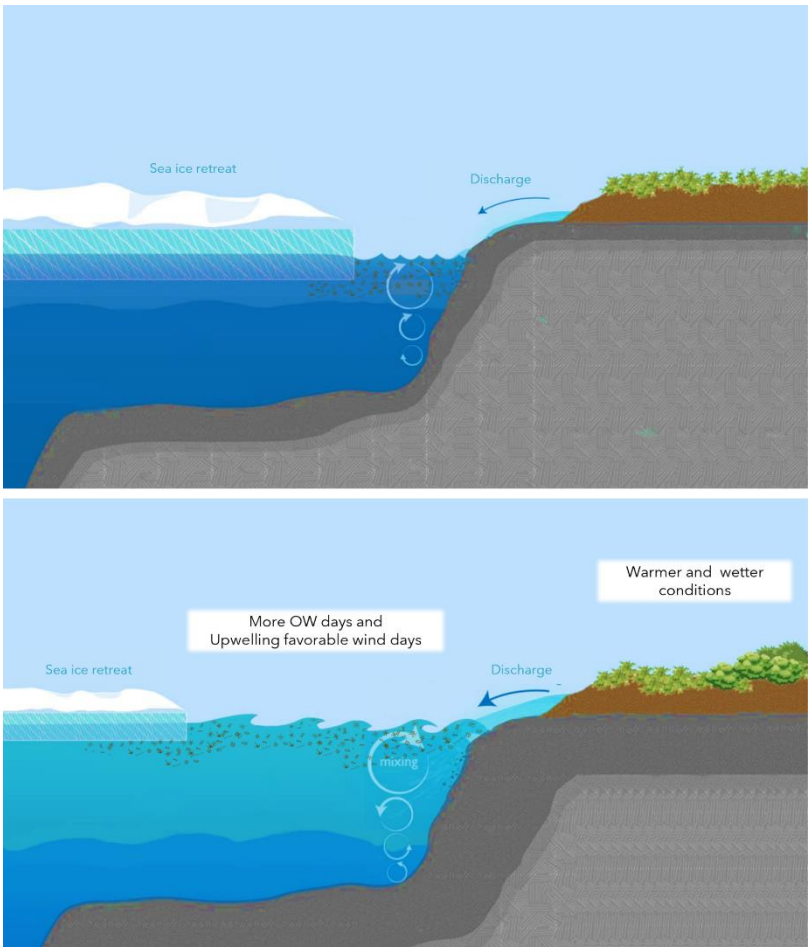

Figure 7. Before (top panel) and after (bottom panel) representation of the Arctic coastal margin as a response to observed warming and increased OW conditions, upwelling favorable wind days, and runoff.

increase along Barents (0.013 m yr-1), reflect alterations in regional hydrology that might influence nutrient availability and thus productivity in the ocean and also seems to potentially suggest added water to the landscape is not reducing terrestrial productivity (Peterson et al., 2006). Nutrient availability is also regulated by the interannual variability in riverine, open, and bottom water supply. For our study area, the influence of riverine discharge during spring and summer and the upwelling of nutrients would dominate. Changes in upwelling favorable wind days, with trends observed along Bering (0.031 d yr^{-1}), Eurasian (0.029 d yr^{-1}), Amerasian (0.052 d yr^{-1}), Barents (0.022 d yr^{-1}), and Okhotsk (0.021 d yr-1), may be indicative of alterations in coastal ocean dynamics affecting productivity (Carmack and Chapman, 2003). The increase in open water days, particularly in regions like the Eurasian coastal margin (0.291 d yr^{-1}), aligns with decreasing sea ice conditions, facilitating more sunlight penetration and thereby boosting marine photosynthesis (Arrigo et al., 2008). The observed increase in marine primary production can also be driven by the continuous supply of nutrients from the Pacific Ocean through the Bering Strait (Popova et al., 2013) and from the North Atlantic to the Barents Sea. Declines in sea ice extent can also potentially increase internal wave energy and erode stratification. Overall, positive trends in LST, SST, P-E, runoff, and upwelling favorable wind days across most sectors have contributed to the increase in productivity, driven by the general warming trend, increasing water availability, and decreasing sea ice conditions (Parkinson, 2014; Bintanja and Selten, 2014).

The observation of varying Coastal Synchrony Index (CSI) values across different Arctic sectors and its relationship with changing environmental conditions show regional dynamics and ecological interconnections. A sector's position on the scatter diagrams in Figure 5, when viewed in light of the CSI, suggests the balance or imbalance between oceanic and terrestrial productivity in response to specific climatic or oceanographic drivers. For instance, sectors with CSI values exceeding 1 in areas like the Barents (4.0), CAA (2.6), and Hudson (2.5) show regional heterogeneity corresponding to areas with the highest rates of change in OW days, runoff, and upwelling favorable wind days. The Barents Sea has been experiencing a pronounced warming trend leading to increased ice-free conditions, thus favoring marine productivity (Polyakov et al., 2020). However, it is worth noting that LST and SST are interestingly not necessarily the direct predictors of CSI, but rather their impact on state conditions. In the CAA, recent changes include shifts in ocean circulation and water mass characteristics, affecting nutrient availability and ocean

GPP (Yamamoto-Kawai et al., 2009). Meanwhile, in the Hudson Bay sector, there has been a marked increase in freshwater runoff, potentially influencing nutrient dynamics, and contributing to changes in ocean productivity (Déry et al., 2005). In contrast, sectors such as Amerasian and B/L, with CSI values below 1, hint at a relatively resilient or slow-changing oceanic system, perhaps due to their ecological, climatic, and geophysical properties that generate more buffering mechanisms. In this study, the CSI metric not only offers a consolidated view of how terrestrial and marine ecosystems interact and are influenced by overarching environmental changes, but it also provides a diagnostic tool for evaluating regional ecosystem shifts.

Given that the Arctic coastal margins are uniquely and vastly sensitive to the timing and presence or absence of sea ice, we first analyzed the coherence of land and ocean primary productivity with each other as well as with the duration of ice-free conditions in nearshore coastal waters. Decomposing ocean GPP and land GPP into the time-frequency space and looking at their cross-wavelet transformation in figure 6a shows that the adjacent land-ocean systems share a common dominant period of 4-5 years. This demonstrates that the synchrony we observed from previous analysis over decadal timescales is mirrored by synchrony on higher frequency timescales. This is also seen in figure 6b, which illustrates the average power, which gives an indication of the strength of the presence of patterns between land and ocean GPP at different periods (years). The ocean GPP (blue) contains a persistent cycle of about 4 years, while the land GPP (red) contains a dominant period of 3-5 years. The OW days (orange) on the other hand also show a dominant period between 4-5 years. This shared 4–5-year period between land and ocean GPP appears to be synchronized with a significant 4-5-year natural oscillation of sea ice in polar areas as also observed by Scafetta & Mazzarella (2015). It is also interesting to note that runoff (green) seems to have a dominant period of 7 years and 2 years. These results could indicate that OW days drive land-ocean GPP synchrony on interannual timescales, while the role of runoff is occurring more strongly over longer timescales.

To assess higher frequency dynamics in coastal synchrony potentially masked by the multidecadal trends captured in the CSI, we conducted a wavelet coherence and cross-wavelet analysis on adjacent land and ocean GPP. The shared dominant period of 4-5 years illustrates that the coastal synchrony observed over decadal timescales is mirrored over interannual timescales. Looking at

the strength of the cycles of land and ocean GPP and OW days, we see a common 4–5-year period, which could indicate that OW days drive the synchrony of land and ocean GPP over interannual timescales. The emergence of shared 4–5-year oscillatory periods in both ocean and land GPP directly corresponds to inherent sea ice dynamics (Scafetta & Mazzarella, 2015). The strong synchrony on the scale of a 4-5-year cycle shared by the parameters observed here indicates that the growing disappearance of shorefast ice not only strongly influences the convergence on adjacent land and ocean primary productivity, but also shares common long-term periodicities with the coastal carbon sink. Interestingly, average power spectra of runoff with a dominant period of 7 years seem to show that its role occurs more strongly over longer timescales.

This study is constrained by the concurrent availability of data over both land and ocean on the years being compared. In addition, the authors have opted to focus on assessing sectoral patterns of primary productivity trends in this study. We recognize the significance of additional factors like coastal erosion, geological characteristics, river runoff, and nutrients, but consistent data for these variables are either sparse or unavailable for the regions and times of interest and are better studied locally in places with intensive measurement strategies. The infrequency of measurements, both temporally and spatially, makes it challenging to accurately constrain net exchanges in coastal ocean settings. Significant uncertainties are also associated with land-derived fluxes, emphasizing the need to comprehend the intricacy of the nutrient budget in this region, particularly along the land-ocean interface. There is also uncertainty associated with remotely sensed observations along the coastal areas. To address uncertainties from the unique bio-optical properties of Arctic coastal waters, the authors utilized primary productivity data from Lewis et al. (2020), along with the traditional ocean primary productivity products that are currently available. The contrasting trends in different products like VGPM, Lewis, and CbPM presented here underline the importance of using multiple data sources to capture the dynamic and multifaceted nature of primary productivity in the pan-Arctic.

5. Conclusions

This study leverages nearly two decades of remote sensing data to analyze large-scale changes in primary production in the Arctic coastal margins, revealing an interconnected picture of marine

and terrestrial environments. The findings show that marine systems in Arctic coastal areas are distinctively more productive than tundra environments, surpassing them by four times. Over the study period of 2003-2020, we learned that GPP along the coastal land and ocean strip has increased by almost the same magnitude of 12%. This indicates that the land-ocean GPP trends along the pan-Arctic coastal margin tend to have expansive or common responses to recent rapid climate change. When looking at the different sectors, the strength and even direction of these trends, a phenomenon we call *Synchronized Positive Shift (SPS)* was observed, showing convergence, and increasing primary productivity over land and ocean across the pan-Arctic coasts, which seem to be a product of increased regional warming. Overall, positive trends in LST, SST, P-E, runoff, and upwelling favorable wind days across most sectors have contributed to the increase in productivity, driven by the general warming trend, increasing water availability, and decreasing sea ice conditions. We observed that inflow margins like Barents, Bering, and Okhotsk, outflow margins like CAA and Greenland/Iceland, as well as interior margins along Eurasia, are sectors where ocean productivity is increasing faster than land productivity. Additionally, the strong coherence on the scale of 4-5-year cycle shared by marine, terrestrial GPP and OW days observed here indicates that the growing disappearance of shorefast ice influences the convergence on adjacent land and ocean primary productivity. As the Arctic coastal areas continue to transition to an ice-free, warmer, and wetter future, it is uncertain whether this SPS pattern between land and ocean GPP along the coastal margins will continue to occur or whether thresholds will be reached where divergence will begin to emerge. We suggest arguing that it is important to integrate the coastal synchrony information developed here as a tool for climate model validation so we can improve our understanding of future trajectories in the coastal Arctic and all the life that it supports.

Open Research

We use FluxSat v2.0 GPP product (Joiner & Yoshida, 2020) over land, which is based on the MCD43C Bidirectional Reflectance Distribution Function (BRDF)-Adjusted reflectance from the Moderate-resolution Imaging Spectroradiometer (MODIS) Terra and Aqua. The GPP product over the ocean is estimated from the Carbon-based Productivity Model (CbPM) Net Primary Productivity (NPP) monthly dataset, which was first described by Behrenfeld et al. (2005) and updated by Westberry et al. (2008). The data products used here are Land Surface Temperature (LST) -from the MODIS Aqua MYD11C3 version 6 data product (Wan et al., 2015) available

from doi.org/10.5067/MODIS/MYD11C3.006, Sea Surface Temperature (SST) also from the MODIS-Aqua (NASA OBPG, 2020) from doi.org/10.5067/MODSA-8D9D4. The P-E and runoff over land, P-E over the ocean, and Wind data are from the European Centre for Medium-Range Weather Forecasts (ECMWF) Reanalysis 5 (ERA5) (Muñoz-Sabater, 2019) from doi.org/10.24381/cds.68d2bb30. For the sea ice concentration data, we used the Bootstrap version 2 (SB2) sea ice data (Comiso et al., 2017) from the National Snow and Ice Data Center (NSIDC) acquired from doi.org/10.5067/7Q8HCCWS4I0R.

References

Arrigo, K. R., & van Dijken, G. L. (2004). Annual changes in sea-ice, chlorophyll a, and primary production in the Ross Sea, Antarctica. Deep Sea Research Part II: Topical Studies in Oceanography, 51(1-3), 117-138.

Arrigo, K. R., van Dijken, G., & Pabi, S. (2008). Impact of a shrinking Arctic ice cover on marine primary production. Geophysical Research Letters, 35(19).

Bakun, A. (1990). Global climate change and intensification of coastal ocean upwelling. Science, 247(4939), 198-201. DOI: 10.1126/science.247.4939.198

Barnhard K. R., Overeem, I., Anderson, S. (2014). The effect of changing sea ice on the physical vulnerability of Arctic coasts. The Cryosphere, 8, 1777-1799. doi:10.5194/tc-8-1777-2014.

Behrenfeld, M.J., & Falkowski, P.G. (1997). A consumer's guide to phytoplankton primary productivity models. Limnology and Oceanography, 42(7), 1479-1491. doi:10.4319/lo.1997.42.7.1479.

Behrenfeld, M. J., E. Boss, D. A. Siegel, and D. M. Shea (2005), Carbon-based ocean productivity and phytoplankton physiology from space, Global Biogeochem. Cycles, 19, GB1006, doi:10.1029/2004GB002299.

Berkelhammer, M. (2019). Synchronous Modes of Terrestrial and Marine Productivity in the North Pacific. Frontiers in Earth Science, Vol 7., ISSN 2296-6463, DOI:10.3389/feart.2019.00073

713 Bhatt US, Walker DA, Raynolds MK, Bieniek PA, Epstein HE, Comiso JC, Pinzon JE, Tucker
714 CJ, Polyakov IV. (2013). Recent Declines in Warming and Vegetation Greening Trends over
715 Pan-Arctic Tundra. *Remote Sensing*, 5(9):4229-4254. https://doi.org/10.3390/rs5094229

716 Bhatt U. S. et al., (2010). Circumpolar Arctic tundra vegetation change is linked to sea ice
717 decline, *Earth Interact.* DOI: 10.1175/2010EI315.1.

718 Bhatt, U. S., Walker, D. A., Raynolds, M. K., Comiso, J. C., Epstein, H. E., Jia, G., ... & Pinzon,
719 J. E. (2014). Circumpolar Arctic tundra vegetation change is linked to sea ice decline. Earth
720 Interactions, 14(8), 1-20.

721 Bhatt U. S. *et al* (2017). Changing seasonality of panarctic tundra vegetation in relationship to
722 climatic variables *Environ. Res. Lett.* 12.

723 Bhatt U.S. *et al* (2021). Climate drivers of Arctic tundra variability and change using an
724 indicators framework. *Environ. Res. Lett.* 16 055019.

725 Bintanja, R., Selten, F. Future increases in Arctic precipitation linked to local evaporation and
726 sea-ice retreat. *Nature* 509, 479–482 (2014). https://doi.org/10.1038/nature13259.

727 Carmack, E. C., Polyakov, I. V., Padman, L., Fer, I., Hunke, E., Hutchings, J., ... & Perovich, D.
728 K. (2015). Toward quantifying the increasing role of oceanic heat in sea ice loss in the new
729 Arctic. Bulletin of the American Meteorological Society, 96(12), 2079-2105.

730 Carmack, E. C., et al. (2016), Freshwater and its role in the Arctic Marine System: Sources,
731 disposition, storage, export, and physical and biogeochemical consequences in the Arctic and
732 global oceans, J. Geophys. Res. Biogeosci., 121, doi:10.1002/2015JG003140.

733 Carmack, E.C., D. Barber, J. Christensen, R. Macdonald, B. Rudels, E. Sakshaug (2006).
734 Climate variability and physical forcing of the food webs and the carbon budget on panarctic
735 shelves, *Prog. Oceanogr,* 10.1016/j.pocean.2006.10.005.

736 Carmack, E., Chapman, D.C.,(2003). Wind-driven shelf/basin exchange on an Arctic shelf: The
737 joint roles of ice cover extent and shelf-break bathymetry. Geophysical Research Letters, 30(14).

738 Chen, C.-T. A., & Borges, A. V. (2009). Reconciling Opposing Views on Carbon Cycling in the
739 Coastal Ocean: Continental Shelves as Sinks and Near-Shore Ecosystems as Sources of
740 Atmospheric CO2. *Deep Sea Research Part II: Topical Studies in Oceanography*, 56, 578-590.
741 https://doi.org/10.1016/j.dsr2.2009.01.001.

742 Clarke, A., & Gaston, K. J. (2006). Climate, energy and diversity. Proceedings of the Royal
743 Society B: Biological Sciences, 273(1599), 2257-2266. https://doi.org/10.1098/rspb.2006.3545.

744 Clow, G. D., DeGange, A. R., Dirksen, D. V., Zimmerman, C. E. (2011). Climate change
745 considerations, in: An Evaluation of the Science Needs to Inform Decisions on Outer Continental
746 Shelf Energy Development in the Chukchi and Beaufort Seas, Alaska, edited by: Holland-
747 Bartels, L. and Pierce, B., US Geological Survey Circular 1370, 81–108, 2011.

748 Comiso, J. C., W. N. Meier, and R. Gersten (2017). Variability and trends in the Arctic Sea ice
749 cover: Results from different techniques. *Journal of Geophysical Research:*
750 *Oceans*, 122 (8): 6883-6900 doi:10.1002/2017jc012768.

751 Cury, P., & Roy, C. (1989). Optimal Environmental Window and Pelagic Fish Recruitment
752 Success in Upwelling Areas. Canadian Journal of Fisheries and Aquatic Sciences, 46(4), 670–
753 680. doi:10.1139/f89-086.

754 Day, J. J., & Hodges, K. I. (2018). Growing land-sea temperature contrast and the intensification
755 of Arctic cyclones. *Geophysical Research*
756 *Letters*, 45, 3673– 3681. https://doi.org/10.1029/2018GL077587

757 Déry, S. J., et al. (2005). Characteristics and trends of river discharge into Hudson, James, and
758 Ungava Bays, 1964–2000. Journal of Climate, 18(14), 2540-2557.

759 DeGrandpre, M. D., Körtzinger, A., Send, U., Wallace, D. W. R., and Bellerby, R. G. J. (2006),
760 Uptake and sequestration of atmospheric CO2 in the Labrador Sea deep convection region,
761 *Geophys. Res. Lett.*, 33, L21S03, doi:10.1029/2006GL026881.

762 Elmendorf, S.C.; Henry, G.H.R.; Hollister, R.D.; Bjork, R.G.; Bjorkman, A.D.; Callaghan, T.V.;
763 Collier, L.S.; Cooper, E.J.; Cornelissen, J.H.C.; Day, T.A.; et al. (2012). Global assessment of
764 experimental climate warming on tundra vegetation: heterogeneity over space and time. Ecol.
765 Lett, 15, 164–175.

766 England, M. R., Eisenman, I., Lutsko, N. J. & Wagner, T. J. (2021). The recent emergence of
767 Arctic Amplification. *Geophys. Res. Lett.* 48, e2021GL094086.

768 Epstein, H. E., Bhatt, U. S., Raynolds, M. K., Walker, D. A., Forbes, B. C., Macias-Fauria, M.,
769 Bjerke, J. (2018). Tundra greenness. In: Arctic Report Card 2018. Retrieved from
770 https://www.arctic.noaa.gov/Report-Card/Report-Card-
771 2018/ArtMID/7878/ArticleID/777/Tundra-Greenness.

772 Farquharson, L.M., D.H. Mann, D.K. Swanson, B.M. Jones, R.M. Buzard, J.W. Jordan (2018).
773 Temporal and spatial variability in coastline response to declining sea-ice in northwest Alaska.
774 Marine Geology, 404 71-83.

775 Fernandez-Mendez, M., C. Katlein, B. Rabe, M. Nicolaus, I. Peeken, K. Bakker, H. Flores, and
776 A. Boetius, (2015). Photosynthetic production in the central Arctic Ocean during the record sea-
777 ice minimum in 2012. Biogeosci., 12, 3525-3549.

778 Frey, K. E., D. K. Perovich, and B. Light. (2011). The spatial distribution of solar radiation under
779 a melting Arctic sea ice cover. Geophysical Research Letters 38, L22501,
780 doi:10.1029/2011GL049421.

781 Frost, G. V., R. A. Loehman, L. B. Saperstein, M. J. Macander, P. R. Nelson, D. P. Paradis, and
782 S. M. Natali. (2020). Multi-decadal patterns of vegetation succession after tundra fire on the
783 Yukon-Kuskokwim Delta, Alaska. Environmental Research Letters. 15(2): 025003.
784 DOI:10.1088/1748-9326/ab5f49.

785 Garcia, C., J. C. Comiso, M. Berkelhammer, and L. Stock (2021). Interrelationships of Sea
786 Surface Salinity, Chlorophyll-α Concentration, and Sea Surface Temperature near the Antarctic
787 Ice Edge. J. Climate, 34, 6069–6086, https://doi.org/10.1175/JCLI-D-20-0716.1.

788 Graham, R. M., L. Cohen, A. A. Petty, L. N. Boisvert, A. Rinke, S. R. Hudson, M. Nicolaus, and
789 M. A. Granskog (2017), Increasing frequency and duration of Arctic winter warming events,
790 Geophys. Res. Lett., 44, doi:10.1002/ 2017GL073395.

791 Harris, P.T., M. Macmillan-Lawler, J. Rupp, E.K. Baker (2014). Geomorphology of the oceans,
792 *Marine Geology*, Volume 352, Pages 4-24, ISSN 0025-3227,
793 https://doi.org/10.1016/j.margeo.2014.01.011.

794 Halsey KH, Milligan AJ, Behrenfeld MJ. 2010. Physiological optimization underlies growth
795 rate-independent chlorophyll-specific gross and net primary production. *Photosynthesis*
796 *Research* 103: 125– 137. DOI 10.1007/s11120-009-9526-z.

797 Irrgang, A.M., Bendixen, M., Farquharson, L.M. et al. (2022). Drivers, dynamics and impacts of
798 changing Arctic coasts. Nat Rev Earth Environ 3, 39–54. https://doi.org/10.1038/s43017-021-
799 00232-1

800 Isaksen, K., Nordli, Ø., Ivanov, B. *et al.* (2022). Exceptional warming over the Barents area. *Sci*
801 *Rep* 12, 9371. https://doi.org/10.1038/s41598-022-13568-5

802 Jakobsson, M. (2002). Hypsometry and volume of the Arctic Ocean and its constituent seas,
803 *Geochem. Geophys. Geosyst.*, 3(1), doi:10.1029/2001GC000302.

804 Jeong, et al. (2018). Accelerating rates of Arctic carbon cycling revealed by long-term
805 atmospheric CO2 measurements

806 Joiner, J., & Yoshida, Y. (2020). Satellite-based reflectances capture large fraction of variability
807 in global gross primary production (GPP) at weekly time scales. *Agricultural and Forest*
808 *Meteorology*, *291*, 108092.

809 Kahru, M., Brotas, V., Manzano-Sarabia, M., & Mitchell, B. G. (2011). Are phytoplankton
810 blooms occurring earlier in the Arctic? Global Change Biology, 17(4), 1733-1739.

811 Kankaanpää, T, Vesterinen, E, Hardwick, B, et al. Parasitoids indicate major climate-induced
812 shifts in arctic communities. *Glob Change*
813 *Biol*. 2020; 26: 6276– 6295. https://doi.org/10.1111/gcb.15297.

814 Kim, YH., Min, SK., Gillett, N.P. et al. (2023). Observationally-constrained projections of an
815 ice-free Arctic even under a low emission scenario. Nat Commun 14, 3139.
816 https://doi.org/10.1038/s41467-023-38511-8

817 Kwok, R. (2002). Sea ice concentration estimates from satellite passive microwave radiometry
818 and openings from SAR ice motion, *Geophys. Res. Lett.*, 29(9), doi:10.1029/2002GL014787.

819 Leu, E., C. J. Mundy, P. Assmy, K. Campbell, T. M. Gabrielsen, M. Gosselin, T. Juul-Pedersen,
820 and R. Gradinger. (2015). Arctic spring awakening - Steering principles behind the phenology of

vernal ice algal blooms. Progress in Oceanography, http://dx.doi.org/10.1016/j.pocean.2015.07.012.

Lewis, K. M., & Arrigo, K. R. (2020). Ocean color algorithms for estimating chlorophyll a, CDOM absorption, and particle backscattering in the Arctic Ocean. Journal of Geophysical Research: Oceans, 125, e2019JC015706. https://doi.org/10.1029/2019JC015706

Lewis, K. M., G. L. van Dijken, and K. R. Arrigo, 2020: Changes in phytoplankton concentration now drive increased Arctic Ocean primary production. Science, 369, 198-202, https://doi.org/10.1126/science.aay8380.

Liu, Y., J. R. Key, Z. Liu, and X. Wang, and S. J. Vavrus (2012), A cloudier Arctic expected with diminishing sea ice, Geophys. Res. Lett., 39, L05705, doi:10.1029/2012GL051251.

Manizza, M., Menemenlis, D., Zhang, H., & Miller, C. E. (2019). Modeling the recent changes in the Arctic Ocean CO2 sink (2006–2013). *Global Biogeochemical Cycles*, 33, 420– 438. https://doi.org/10.1029/2018GB006070.

McNicol, G., Hood, E., Butman, D. E., Tank, S. E., Giesbrecht, I. J. W., Floyd, W., et al. (2023). Small, coastal temperate rainforest watersheds dominate dissolved organic carbon transport to the northeast Pacific Ocean. *Geophysical Research Letters*, 50, e2023GL103024. https://doi.org/10.1029/2023GL103024

Muller-Karger, F.E., Varela, R., Thunell, R., Luerssen, R., Hu, C. and Walsh, J.J. (2005). The importance of continental margins in the global carbon cycle. *Geophysical Research Letters 32: doi: 10.1029/2004GL021346. issn: 0094-8276.*

NASA Ocean Biology Processing Group (OBPG) and R.P. Stumpf. (2012). Distance to Nearest Coastline: 0.01-Degree Grid: Land. Distributed by the Pacific Islands Ocean Observing System (PacIOOS). http://pacioos.org/metadata/dist2coast_1deg_land.html. Accessed 01 January 2021.

National Snow & Ice Data Center (September 21, 2020). *Arctic sea ice decline stalls out at second lowest minimum.* Retrieved from: https://nsidc.org/arcticseaicenews/2020/09/?submit=GO&keywords=2022#:~:text=September%2016%2C%202020%20In%20the%20first%20week%20of,second%20lowest%E2%80%94after%202012%E2%80%94in%20the%2042-year%20continuous%20satellite%20record.

National Snow & Ice Data Center (2021). Sea Ice Index, Version 3. National Snow and Ice Data Center. doi: 10.7265/N5736NV7

NASA MODIS-Aqua Level 3 SST Thermal IR 8-day 9km Daytime v2014.0. doi.org/10.5067/MODSA-8D9D4. PO.DAAC, CA, USA. Dataset accessed: 15 November 2021.

Nishioka, J., Mitsudera, H., Yasuda, I., Liu, H., Nakatsuka, T., and Y. N. Volkov. (2014). Biogeochemical and physical processes in the Sea of Okhotsk and the linkage to the Pacific Ocean, *Progress in Oceanography*, Volume 126, Pages 1-7, ISSN 0079-6611, https://doi.org/10.1016/j.pocean.2014.04.027.

Nummelin, A., Ilicak, M., Li, C., and Smedsrud, L. H. (2016), Consequences of future increased Arctic runoff on Arctic Ocean stratification, circulation, and sea ice cover, *J. Geophys. Res. Oceans*, 121, 617– 637, doi:10.1002/2015JC011156.

McIlhattan, E. A., Kay, J. E., & L'Ecuyer, T. S. (2020). Arctic clouds and precipitation in the Community Earth System Model version 2. *Journal of Geophysical Research: Atmospheres*, *125*, e2020JD032521. https://doi.org/10.1029/2020JD032521.

McLaughlin, F.A & E. C. Carmack, (2010). Deepening of the nutricline and chlorophyll maximum in the Canada Basin interior, 2003-2009. *Geophys. Res. Lett*. 37, L24602. https://doi.org/10.1029/2010GL045459.

Minke, M., Donner, N., Karpov, N., De Klerk, P., and Joosten, H. (2007). Distribution, diversity, development and dynamics of polygons mires: Examples from Northeast Yakutia (Siberia), Peatlands Int., 1, 36–40.

Moritz, S., & Bartz-Beielstein, T. (2017). imputeTS: Time Series Missing Value Imputation in R. *R J.*, *9*, 207.

Muñoz-Sabater, J. (2019). ERA5-Land monthly averaged data from 1981 to present, Copernicus Climate Change Service (C3S) Climate Data Store (CDS) [data set], https://doi.org/10.24381/cds.68d2bb30.

Parkinson, C.L., (2014). Spatially mapped reductions in the length of the Arctic sea ice season. Geophysical Research Letters, 41(12), pp.4316-4322.

877 Popova, E. E., Yool, A., Coward, A. C., Dupont, F., Deal, C., Elliott, S., Hunke, E., Jin,
878 M., Steele, M., and Zhang, J. (2012), What controls primary production in the Arctic Ocean?
879 Results from an intercomparison of five general circulation models with biogeochemistry, *J.*
880 *Geophys. Res.*, 117, C00D12, doi:10.1029/2011JC007112.

881 Peterson, B.J., McClelland, J., Curry, R., Holmes, R.M., Walsh, J.E., Aagaard, K., (2006).
882 Trajectory shifts in the Arctic and subarctic freshwater cycle. Science, 313(5790), pp.1061-1066.

883 Polyakov, I. V., et al. (2020). Greater role for Atlantic inflows on sea-ice loss in the Eurasian
884 Basin of the Arctic Ocean. Science, 356(6335), 285-291.

885 Popova, E. E., Yool, A., Aksenov, Y., and Coward, A. C. (2013), Role of advection in Arctic
886 Ocean lower trophic dynamics: A modeling perspective, *J. Geophys. Res.*
887 *Oceans*, 118, 1571– 1586, doi:10.1002/jgrc.20126.

888 Post, E., Bhatt, U. S., Bitz, C. M., Brodie, J. F., Fulton, T. L., Hebblewhite, M., ... & Walker, D.
889 A. (2013). Ecological consequences of sea-ice decline. Science, 341(6145), 519-524.

890 Post, E., Forchhammer, M. C., Bret-Harte, M. S., Callaghan, T. V., Christensen, T. R., Elberling,
891 B., & Aastrup, P. (2009). Ecological dynamics across the Arctic associated with recent climate
892 change. Science, 325(5946), 1355-1358.

893 Radic´, V. & Hock, R. (2010). Regional and global volumes of glaciers derived from statistical
894 upscaling of glacier inventory data. J. Geophys. Res. 115 10.1029/2009JF001373.

895 Rantanen, M., Karpechko, A.Y., Lipponen, A. *et al.* (2022) The Arctic has warmed nearly four
896 times faster than the globe since 1979. *Commun Earth Environ* 3, 168.
897 https://doi.org/10.1038/s43247-022-00498-3

898 Rawlins, M. A., Steele, M., Holland, M. M., Adam, J. C., Cherry, J. E., Francis, J. A., ... &
899 Peterson, D. L. (2010). Analysis of the Arctic system for freshwater cycle intensification:
900 Observations and expectations. Journal of Climate, 23(21), 5715-5737.

901 Raynolds, M.K., D A. Walker, A. Balser, C. Bay, et al., (2019). A raster version of the
902 Circumpolar Arctic Vegetation Map (CAVM), *Remote Sensing of Environment*, Volume 232,
903 2019, 111297, ISSN 0034-4257, https://doi.org/10.1016/j.rse.2019.111297.

Reynolds, J. F. & Tenhunen, J. D. 1996: Landscape function and disturbance in Arctic tundra. Ecol. Stud. 120. Berlin: Springer.

Rodriguez-Iturbe, I. (2000). Ecohydrology: a hydrologic perspective of climate-soil-vegetation dynamics. Water Resources Research, 36(1), 3-9. https://doi.org/10.1029/1999WR900210.

Rösch, A., & Schmidbauer, H. (2018), WaveletComp: Computational Wavelet Analysis, R Package Version 1.1, https://CRAN.R-project.org/package=WaveletComp.

Scafetta, N. & A. Mazzarella. (2015). The Arctic and Antarctic Sea Ice Area Index Records versus Measured and Modeled Temperature Data. *Advances in Meteorology,* Vol 2015, 481834, https://doi.org/10.1155/2015/481834.

Schuur, E. A. G., McGuire, A. D., Schädel, C., Grosse, G., Harden, J. W., Hayes, D. J., ... & Natali, S. M. (2015). Climate change and the permafrost carbon feedback. Nature, 520(7546), 171-179.

Schuur, E. A. G., Bockheim, J., Canadell, J. G., Euskirchen, E., Field, C. B., Goryachkin, V., Hagemann, S., Kuhry, P., Lafleuar, P. M., Lee, H., Mazhitova, G., Nelson, F. E., Rinke, A., Romanovsky, V. E., Shiklomanov, N., Tarnocai, C., Venevsky, S., Vogel, J. G., and Zimov, S. A., 2008: Vulnerability of permafrost carbon to climate change: implications for the global carbon cycle. BioScience, 58: 701–714.

Serreze, M. C., Barrett, A. P., Slater, A. G., Woodgate, R. A., Aagaard, K., Lammers, R. B., Steele, M., Moritz, R., Meredith, M., and Lee, C. M. (2006), The large-scale freshwater cycle of the Arctic, *J. Geophys. Res.*, 111, C11010, doi:10.1029/2005JC003424.

Serreze, M. C., & Stroeve, J. (2015). Arctic sea ice trends, variability and implications for seasonal ice forecasting. Philosophical Transactions of the Royal Society A: Mathematical, Physical and Engineering Sciences, 373(2045), 20140159.

Serreze, M.C., Barry, R.G., 2011. Processes and impacts of Arctic amplification: A research synthesis. Global and Planetary Change, 77(1-2), pp.85-96.

Slagstad, D., Ellingsen, I. H., & Wassmann, P. (2011). Evaluating primary and secondary production in an Arctic Ocean void of summer sea ice: An experimental simulation approach. Progress in Oceanography, 90(1-4), 117-131.

Stow, D.A., A. Hope, D. McGuire, D. Verbyla., et al. (2003). Remote sensing of vegetation and land-cover change in Arctic Tundra Ecosystems. *Remote Sensing of Environment,* 89, 281-308. doi:10.1016/j.rse.2003.10.018.

Terhaar, J., Lauerwald, R., Regnier, P. *et al.* Around one third of current Arctic Ocean primary production sustained by rivers and coastal erosion. *Nat Commun* 12, 169 (2021). https://doi.org/10.1038/s41467-020-20470-z.

Thomas, D.N., Dieckmann, G.S., 2010. Antarctic Sea Ice–a Habitat for Extremophiles. Science, 295(5555), pp.641-644.

Torrence, C., & Compo, G. (1998). A practical guide to wavelet analysis. *Bulletin of the American Meteorological Society, 79,* 61–78.

Tremblay, J. É., Anderson, L. G., Matrai, P., Coupel, P., Bélanger, S., Michel, C., & Reigstad, M. (2015). Global and regional drivers of nutrient supply, primary production and CO2 drawdown in the changing Arctic Ocean. *Progress in Oceanography, 139,* 171–196. https://doi.org/10.1016/j.pocean.2015.08.009

Steele, M. (2004). Ocean–sea ice interactions: a review. In Sea Ice: An Introduction to its Physics, Chemistry, Biology and Geology (pp. 173-205). Blackwell Publishing Ltd.

Walker, D.A., Raynolds, M.K., Daniëls, F.J., Einarsson, E., Elvebakk, A., Gould, W.A., Katenin, A.E., Kholod, S.S., Markon, C.J., Melnikov, E.S., Moskalenko, N.G., Talbot, S.S., Yurtsev, B.A. and The other members of the CAVM Team, (2005), The Circumpolar Arctic vegetation map. Journal of Vegetation Science, 16: 267-282. https://doi.org/10.1111/j.1654-1103.2005.tb02365.x

Wan, Z., Hook, S., Hulley, G. (2021). MODIS/Aqua Land Surface Temperature/Emissivity Monthly L3 Global 0.05Deg CMG V061 [Data set]. NASA EOSDIS Land Processes DAAC. Accessed 2022-09-12 from https://doi.org/10.5067/MODIS/MYD11C3.061.

Ward, N. et al. (2020). Representing the function and sensitivity of coastal interfaces in Earth system models. *Nature Communications* 11: 1–14.

Wassmann, P., Duarte, C.M., Agustí, S., Sejr, M.K., (2011). Footprints of climate change in the Arctic marine ecosystem. Global Change Biology, 17(2), pp.1235-1249.

Westberry, T., Behrenfeld, M. J., Siegel, D. A., and Boss, E. (2008), Carbon-based primary productivity modeling with vertically resolved photoacclimation, *Global Biogeochem. Cycles*, 22, GB2024, doi:10.1029/2007GB003078.

Yamamoto-Kawai, M., McLaughlin, F. A., Carmack, E. C., Nishino, S., & Shimada, K. (2009). Aragonite undersaturation in the Arctic Ocean: Effects of ocean acidification and sea ice melt. Science, 326(5956), 1098-1100.

Zhang, J., Spitz, Y. H., Steele, M., Ashjian, C., Campbell, R., Berline, L., & Matrai, P. (2010). Modeling the impact of declining sea ice on the Arctic marine planktonic ecosystem. *Journal of Geophysical Research: Oceans*, *115*(10), 1–24. https://doi.org/10.1029/2009JC005387.

Zhang, X., Sun, S., Xie, H., Liu, Y., Shao, D., & Qin, B. (2013). Effects of warming on chlorophyll degradation and carbohydrate accumulation of alpine herbaceous species during plant senescence on the Tibetan Plateau. PLoS One, 8(9), e77156.

Zimov, S. A., et al. (2006), Permafrost and the global carbon budget, *Science*, 312, 1612 – 1613